Selective Laser Melting Additive Manufacturing of Ti-Based Nanocomposites: The Role of Nanopowder

DONGDONG GU, HONGQIAO WANG, and GUOQUAN ZHANG

The additive manufacturing of bulk-form TiC/Ti nanocomposite parts was performed using Selective Laser Melting (SLM). Two categories of nanopowder, *i.e.*, ball-milled TiC/Ti nanocomposite powder and directly mechanical mixed nano-TiC/Ti powder, were used for SLM. The influences of nanopowder characteristics and laser processing parameters on the densification behavior, microstructural features, and tribological properties of the SLM-processed TiC/Ti nanocomposite parts were studied. The study showed that the densification of TiC/Ti nanocomposite parts was affected by both laser energy density and powder categories. Using an insufficient laser energy density of 0.25 kJ/m lowered SLM densification rate, because of the occurrence of balling effect. An increase in the laser energy density above 0.33 kJ/m produced near fully dense SLM parts. The SLM densification levels of the ball-milled TiC/Ti nanocomposite powder were generally higher than that of the directly mixed nano-TiC/Ti powder. The TiC-reinforcing phase in SLM-processed TiC/Ti parts typically had a lamellar nanostructure with a nanoscale thickness, completely differing from the starting nanoparticle morphology before SLM. The lamellar nanostructure of the TiC reinforcement in SLM-processed ball-milled TiC/Ti nanocomposite parts could be maintained within a wide range of laser energy densities. However, the microstructures of the SLM-processed, directly mixed nano-TiC/Ti powder were sensitive to SLM parameters, and the TiC reinforcement experienced a successive change from the lamellar nanostructure to the relatively coarsened dendritic microstructure as laser energy density increased. A combination of the sufficiently high SLM densification rate and the formation of the nanostructured TiC reinforcement favored the improvement of the tribological property, leading to the considerably low coefficient of friction of 0.22 and wear rate of 2.8×10^{-16} m^3 N^{-1} m^{-1}. The coarsening and resultant disappearance of nanoscale TiC reinforcement in SLM-consolidated directly mixed nano-TiC/Ti powder at a high laser energy density lowered the tribological performance considerably.

DOI: 10.1007/s11661-013-1968-4

I. INTRODUCTION

SELECTIVE Laser Melting (SLM), as the newly developed additive manufacturing (AM) technology, enables realizing quick production of three-dimensional parts with any complex configurations directly from powders.[1–3] Unlike the conventional material-removal processing method, SLM is based on a completely opposite philosophy, *i.e.*, material incremental manufacturing (MIM).[4–10] SLM creates components in a layer-by-layer manner by selective fusion and consolidation of thin layers of loose powder, using a high-energy laser beam. SLM process, accordingly, has a number of advantages such as net-shape fabrication without the requirement of molds or dies, a high level of process flexibility, and a wide range of applicable materials.[11–15] SLM typically involves a unique non-equilibrium physical metallurgical nature. A high-energy laser beam can be focused to a power density up to 10^{10-12} W/cm^2 during SLM, and can heat a material surface rapidly to a temperature up to 10^5 K, followed by a rapid cooling at a rate up to 10^{6-7} K/s.[16,17] It thus provides a high potential for obtaining very fine microstructures with superior metallurgical properties.

In recent years, the introduction of SLM in processing the novel nanomaterial components has attracted growing interest in the research fields of AM.[3,18,19] Starting from the nanoscale powders, SLM has created new technological opportunities for manufacturing bulk-form nanomaterial components with unique nanostructures and properties, because of the combination of special MIM production strategy and highly nonequilibrium metallurgical process of SLM.[20,21] Nevertheless, as a primary difficulty associated with the bulk-form components condensed from ultrafine nanopowder, the uncontrolled agglomeration of nanoparticles due to the considerably large van der Waals attractive force between neighboring particles may result in the microstructural inhomogeneity, and even the disappearance of original favorable nanostructures.[22–25] In a more serious situation, the nonuniform microstructures are directly related to the formation of differential

DONGDONG GU, Professor, HONGQIAO WANG, and GUOQUAN ZHANG, Graduate Students, are with the College of Materials Science and Technology, Nanjing University of Aeronautics and Astronautics (NUAA), 210016 Nanjing, P.R. China. Contact e-mail: dongdonggu@nuaa.edu.cn
Manuscript submitted August 26, 2012.
Article published online September 6, 2013

stresses and resultant propagation of internal cracks in consolidated parts, which is regarded as a key factor in influencing the densification behavior of bulk-form nanomaterial components.[26–29] Therefore, the primary goal of SLM is to enhance the dispersion homogeneity of the strongly interacting nanoparticles and attendant densification response. SLM, as implied in its name, is processed, based on a metallurgical mechanism of the full melting and subsequent rapid solidification. Significant understanding is, thus, required to study how the nanostructures are crystallized and developed during SLM process with a complete liquid formation. The underlying roles of starting-powder characteristics and SLM processing parameters employed in the formation and controllability of nanostructures in the SLM route should be clarified.

Nowadays, there is considerable interest in the development of particle-reinforced Ti matrix composites (TMCs) due to its isotropic characteristics and excellent combination of strength-to-weight ratio and high-temperature properties as well as its low cost compared with the continuously reinforced TMCs.[30] TMCs, accordingly, have the promising potential applications in the aeronautical, astronautical, and chemical industries. Among the reinforcements introduced to TMCs, TiC and TiB are considered the most suitable because of the high modulus, high thermal stability, similar density, and chemical compatibility with Ti.[31] Recently, we have performed the preliminary attempts for SLM fabrication of nanoscale TiC-reinforced Ti matrix nanocomposite parts.[32,33] As SLM starts from the nanopowder to create bulk-form parts, the characteristics of the starting nanopowder, *e.g.*, particle morphology, particle size, and powder dispersion state, played a substantial role in determining the nanostructures of TiC reinforcement in the SLM-processed parts. Moreover, the densification response, nanostructural features, and mechanical properties of the SLM-processed nanocomposites are dependent on laser-processing conditions. Therefore, the relationship between nanopowder, SLM process, and laser processability needs to be determined.

In the current study, SLM was applied to process TiC/Ti nanocomposite powder prepared using two different methods, *i.e.*, ball-milling method and directly mechanical mixing method. The evolutions of nanostructures of SLM-processed TiC/Ti nanocomposite parts at different laser processing parameters were studied and the attendant densification level and tribological property were assessed. The predominant roles of the starting nanopowder characteristics and the corresponding SLM parameters in the variations in microstructural and mechanical properties were clarified.

II. EXPERIMENTAL PROCEDURES

A. *Powder Preparation*

The flowability of the powder is of primary importance for the powder-bed-based SLM process, which further requires that the powder particles have the uniform structure and size distribution.[3,34] In this study, the TiC/Ti nanocomposite powder used for SLM was prepared by the following two different methods.

1. *First kind of TiC/Ti nanocomposite powder: prepared by ball milling of micronsized TiC and Ti powders*

The starting powder components included 99.7 pct purity TiC powder with an irregular shape and a mean particle size of 1.5 μm (Figure 1(a)) and 99.9 pct purity Ti powder with an irregular structure and an average particle size of 45 μm (Figure 1(b)). The TiC and Ti constituents were mixed according to a weight ratio of 15:85. Ball milling of TiC/Ti mixture was performed in a high-energy Pulverisette 6 planetary mono-mill (Fritsch GmbH, Germany). The stainless steel grinding balls and the powder mixture to be ground were charged into a hardened chromium steel grinding bowl, with the ball-to-powder weight ratio of 10:1. Before the formal powder preparation, one batch of TiC/Ti powder was pre-milled in the grinding bowl with the grinding balls for 2 hours, in order to clean the grinding media and decrease the iron or other contamination. The whole powder-handling and milling process was under the protection of argon atmosphere to decrease the detrimental influence of oxygen and nitrogen. The rotation speed of the main disk was fixed at 250 rpm, and the milling time was optimized at 10 hours. In order to avoid excessive temperature rise within the grinding bowl, 20 minutes of ball milling was followed by 10 minutes interval. The milled TiC/Ti composite powder had a flattened and angular structure and a uniform particle size distribution, with an average value of 5.8 μm (Figure 1(c)). The selected area diffraction pattern (SADP) of the milled powder revealed the existence of TiC and Ti constitution phases (Figure 1(e)). The bright field transmission electron microscopy (TEM) micrograph showed that the ultrafine nanoscale TiC particulates with a mean size below 50 nm were dispersed uniformly throughout the Ti matrix (Figure 1(d)), thus confirming the formation of TiC_P/Ti nanocomposite powder after ball milling.

2. *Second kind of TiC/Ti nanocomposite powder: prepared by directly mechanical mixing of TiC nanopowder and micronsized Ti powder*

The 99.0 pct purity TiC nanopowder with a spherical shape and a mean particle size of 50 nm (Figure 2(a)) and the 99.7 pct purity Ti powder with a spherical shape and an average particle diameter of 22.5 μm (Figure 2(b)) were used. The TiC/Ti nanocomposite powder consisting of 15 wt pct TiC was mechanically mixed in a Pulverisette 4 vario-planetary mill (Fritsch GmbH, Germany). The rotational speeds of supporting disk and grinding bowls were adjusted at 200 rpm and −250 rpm, respectively, and the mixing duration was settled at 4 hours. The ultrafine TiC nanoparticles were dispersed uniformly around Ti particles surface after the mechanical mixing process (Figure 2(c)). In contrast with the ball-milling process, the powder particles did not experience any deformation and structural change during the mixing process. The spherical Ti powder particles were

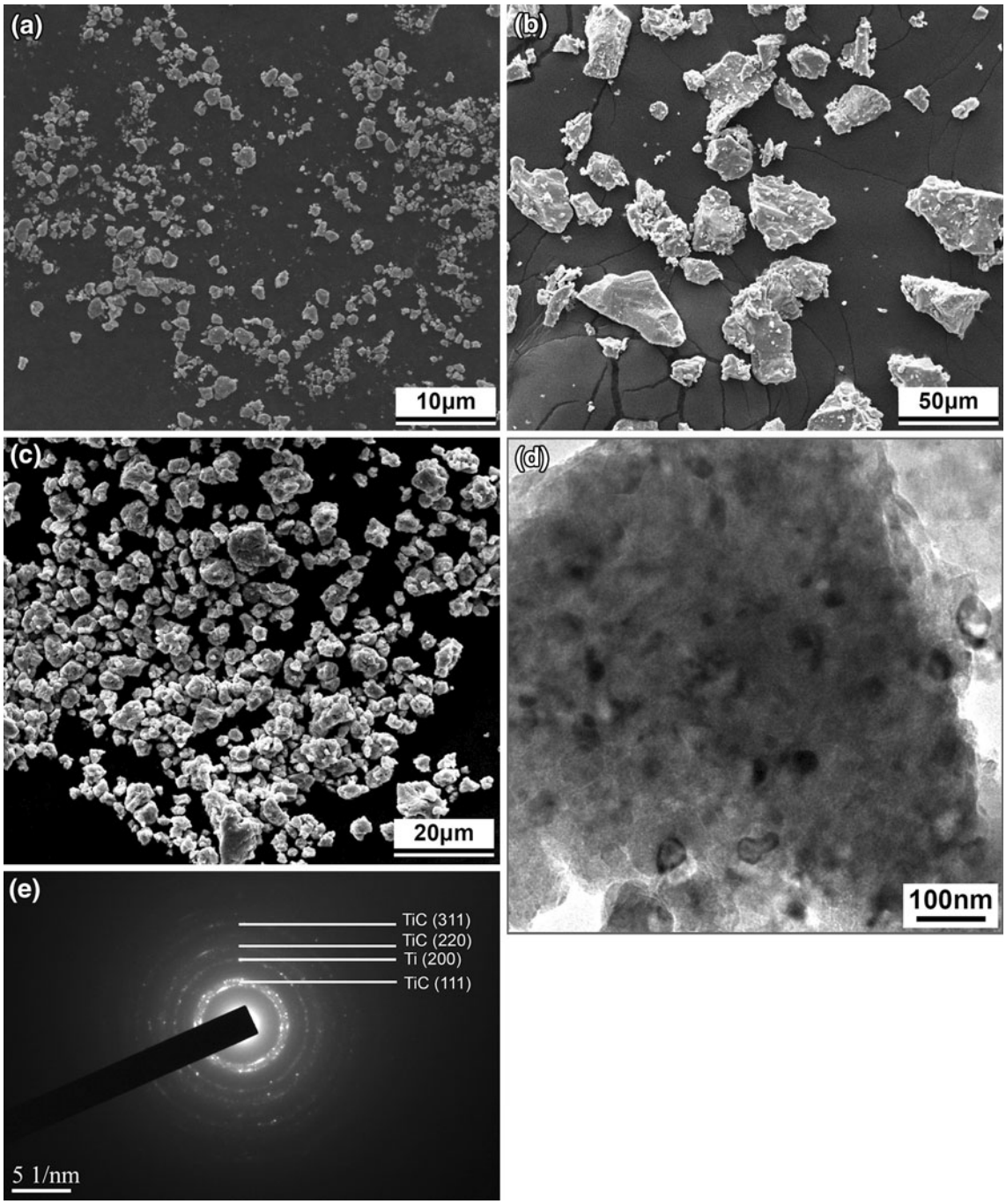

Fig. 1—Preparation of the first kind of TiC/Ti nanocomposite powder by ball milling: The starting micronsized TiC (*a*) and Ti (*b*) powder (SEM); (*c*) ball-milled TiC/Ti composite powder particles (SEM); (*d*) TEM micrograph showing the dispersion of TiC nanoparticles within the interior Ti matrix; (*e*) SADP showing the existence of TiC and Ti constitution phases.

accordingly used, in order to obtain a sound flowability of the mixed TiC/Ti nanocomposite powder.

B. *Laser Processing*

The SLM apparatus, as schematically depicted in Figure 3(a), consisted mainly of a YLR-200 Ytterbium fiber laser with a power of ~200 W and a spot size of 70 μm (IPG Laser GmbH, Germany), an automatic powder layering mechanism, an inert argon gas protection system, and a computer system for process control. The real-time SLM process is illustrated in Figure 3(b). First, a Ti substrate was fixed on the building platform and levelled. The building chamber was then sealed and the argon gas with an outlet pressure of 30 mbar was fed inside, decreasing the O_2 content below 10 ppm. Afterward, a thin layer of the powder with a thickness of 50 μm was deposited on the substrate by the layering mechanism. The laser beam then scanned the powder

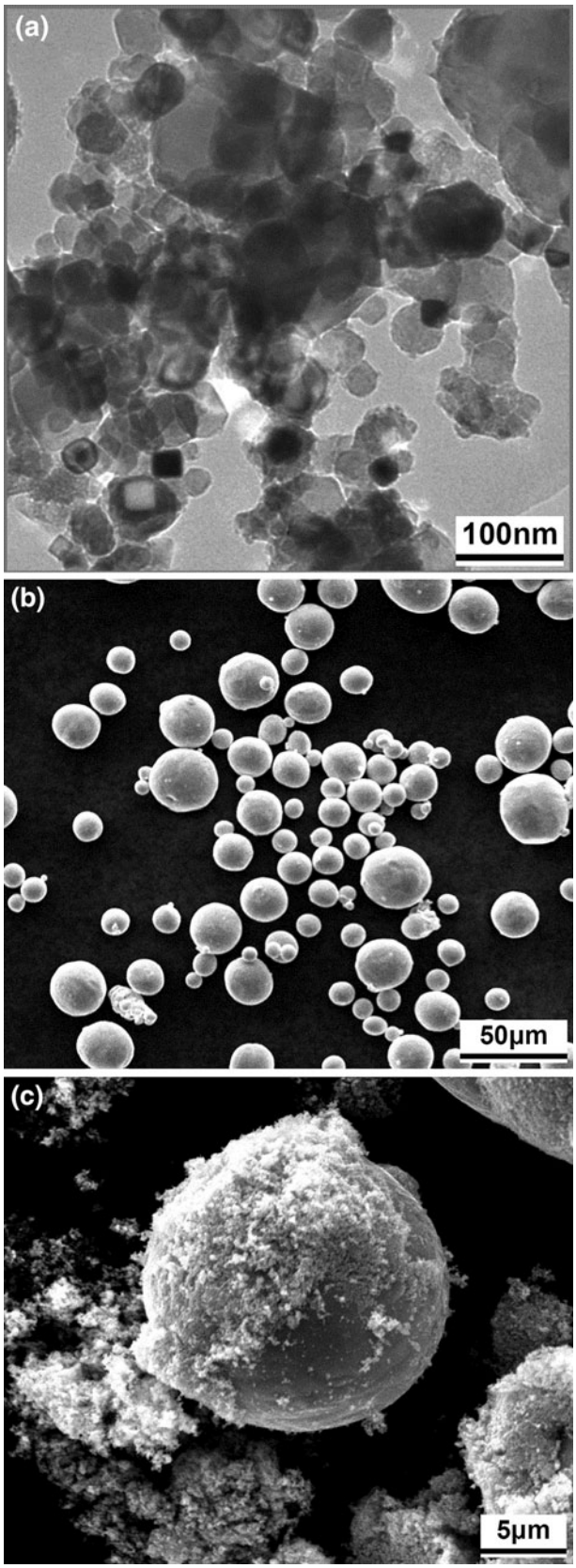

Fig. 2—Preparation of the second kind of TiC/Ti nanocomposite powder by directly mechanical mixing: The starting nanoscale TiC powder (TEM) (*a*) and micronsized Ti powder (SEM) (*b*); (*c*) Uniformly mixed nano-TiC/Ti composite powder (SEM).

bed surface to form a two-dimensional profile according to computer-aided design data of the specimens. A simple linear raster scan pattern was used, with a scan vector length of 4 mm and a hatching spacing of 50 μm. The above process was repeated and the specimens were built in a layer-by-layer manner until completion. The number of layers that was added on the substrate was 160. Cubic specimens with dimensions of 8 mm × 8 mm × 8 mm were prepared. Through a number of preliminary SLM experiments, the laser power (P) was optimized at 100 W. Meanwhile, the scan speeds (v) were settled periodically at 0.1, 0.2, 0.3 and 0.4 m/s by SLM control program. Four different ''linear laser energy densities'' (λ) of 1, 0.5, 0.33, and 0.25 kJ/m, which were defined by $\lambda = P/v$,[35] were used to estimate the laser energy input to the powder being processed.

C. *Microstructural and Mechanical Properties Characterization*

Samples for metallographic examinations were cut, ground, and polished according to the standard procedures, and etched with a solution comprising HF (2 mL), HNO_3 (4 mL), and distilled water (94 mL) for 20 seconds. Low-magnification microstructures and surface morphologies of SLM-processed specimens were characterized using a PMG3 optical microscope (OM) (Olympus Corporation, Japan) and a Quanta 200 scanning electron microscope (SEM) (FEI Company, The Netherlands) in a secondary electron mode at 20 kV. High-resolution study of ultrafine nanostructures was performed using a LEO 1550 field emission SEM (FE-SEM) (Carl Zeiss NTS GmbH, Germany) at 5 kV. The density (ρ) of SLM-processed specimens was measured based on the Archimedes principle. The tribological property of specimens was estimated by dry sliding wear tests conducted in a HT-500 ball-on-disk tribometer (Lanzhou ZhongKe KaiHua Sci. & Technol. Co., Ltd., China) in air at room temperature. Surfaces of samples were ground and polished prior to wear tests. A Φ3 mm GCr15 bearing steel ball having a mean hardness of HRC60 was taken as the counterface material and a test load of 3 N was applied. The friction unit was rotated at a speed of 560 rpm for 30 minutes, with the rotation radius of 2 mm. The coefficient of friction (COF) of the specimens was recorded during wear tests. The wear volume (V) was determined gravimetrically using $V = M_{\text{loss}}/\rho$, where M_{loss} was the weight loss of the samples after wear tests. The wear rate (ω) was calculated by $\omega = V/(WL)$, where W was the contact load and L was the sliding distance.

III. RESULTS

A. *Densification Behavior*

Figure 4 depicts the influences of powder preparation method and laser processing parameters on densification rates of SLM-processed TiC/Ti nanocomposite powder. A close comparison revealed that for a given laser energy density (λ), the SLM densification level of the

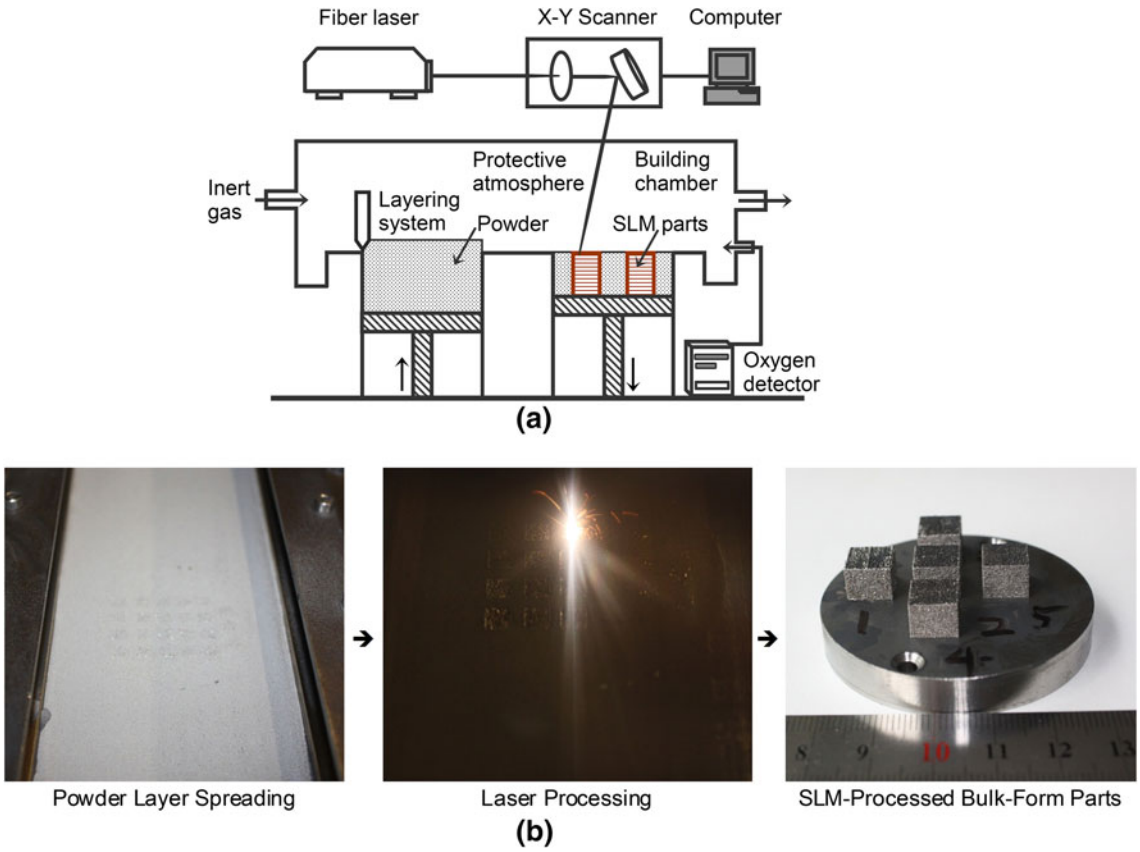

Fig. 3—Schematic of SLM apparatus (*a*); SLM procedure for fabricating bulk-form Ti-based nanocomposite parts (*b*).

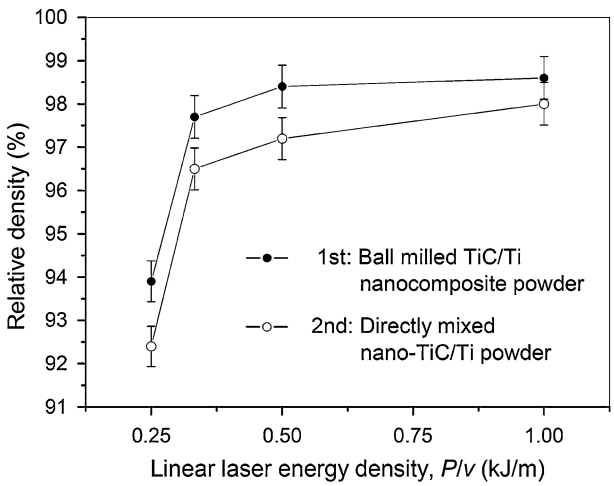

Fig. 4—Variations of SLM densities of TiC/Ti nanocomposite parts with powder categories and SLM processing parameters.

ball-milled TiC/Ti nanocomposite powder was generally larger than that of the directly mixed nano-TiC/Ti powder, typically showing an improvement of 0.6 to 1.5 pct theoretical density (TD). For both the powder systems, the SLM densification rate increased sharply from ~93 pct TD to ~97 pct TD as λ increased from 0.25 to 0.33 kJ/m. A further elevation of the applied λ led to a slight increase in the obtained SLM density. As a sufficiently high λ of 1.0 kJ/m was used, the almost fully dense (>98 pct TD) TiC/Ti nanocomposite parts were generally produced after SLM.

Figures 5 and 6 show respectively the characteristic microstructures on the untreated top surfaces and polished/etched cross sections of SLM-processed parts using ball-milled and directly mixed TiC/Ti nanocomposite powders. At a relatively high laser energy density (λ) of 1.0 kJ/m, the top surface of SLM-processed part using ball-milled TiC/Ti nanocomposite powder was fully dense and smooth, free of any apparent pores (Figure 5(a)). The corresponding cross section of the part typically showed a layered microstructure, due to the AM nature of SLM. The layers were coherently bonded, without the formation of interlayer pores or cracks (Figure 5(c)). As a low λ of 0.25 kJ/m was applied, the SLM-processed surface consisted of interrupted, large-sized agglomerates, between which the open pore channels were visible. Furthermore, a number of metallic balls with an average diameter of ~70 μm were present on the porous surface (Figure 5(b)). It was accordingly concluded that the "balling" effect, which was regarded as a typical metallurgical defect with SLM process,[36–39] occurred in this instance. As a consequence, the cross section consisted of irregular shaped interlayer pores on a scale of ~300 μm (Figure 5(d)), which resulted in a significant decrease in the obtained densification rate (Figure 4).

Basically, the changes of densification behavior and microstructural features of the second kind of directly mixed TiC/Ti nanocomposite powder with SLM

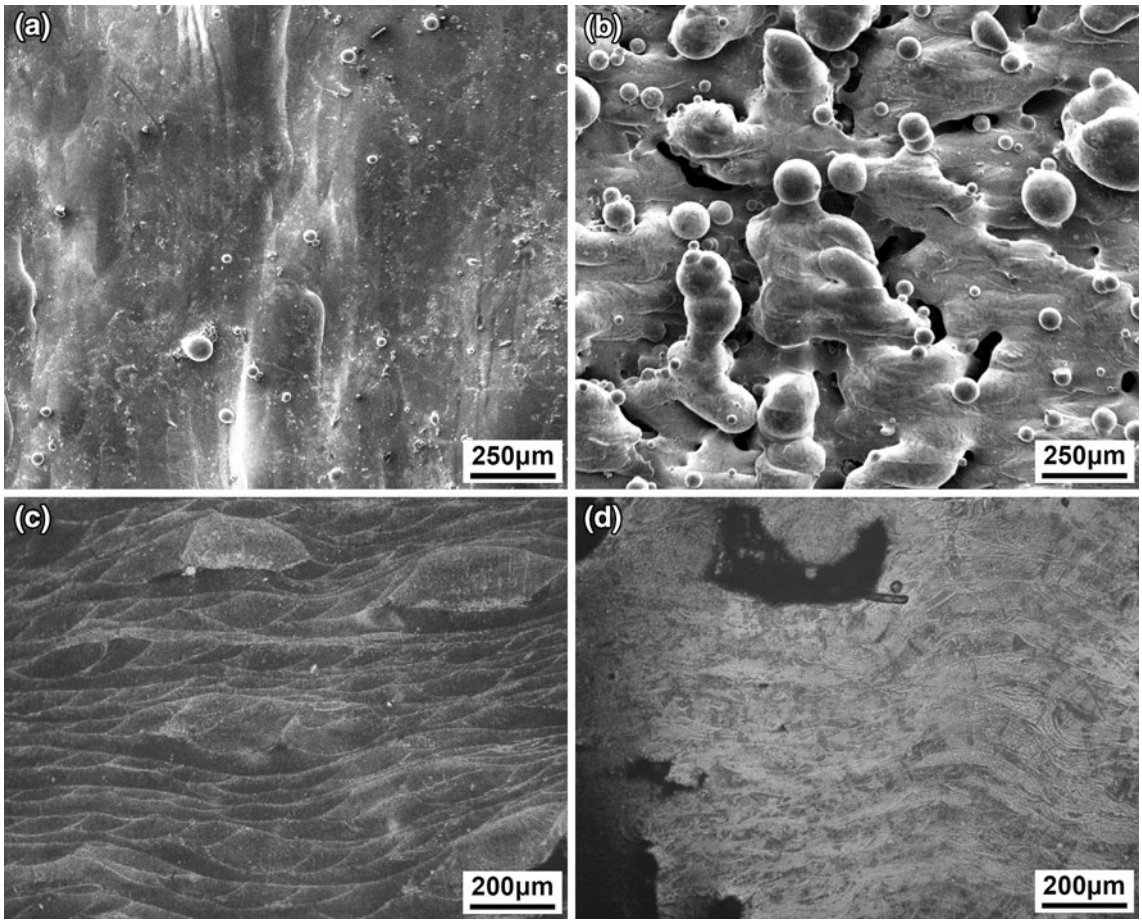

Fig. 5—Typical surface morphologies (SEM) and cross-sectional microstructures (OM) of SLM-processed parts using first kind of ball-milled TiC/Ti nanocomposite powder: $\lambda = 1.0$ kJ/m, $v = 0.1$ m/s (*a* and *c*); $\lambda = 0.25$ kJ/m, $v = 0.4$ m/s (*b* and *d*).

processing parameters showed a similar tendency to that of the first kind of powder. A close examination of microstructures, however, disclosed some distinct differences due to the change in the starting nanopowder. At a relatively high λ of 1.0 kJ/m, although the top surface of the SLM-processed part remained dense (Figure 6(a)), a small amount of micropores were present on the cross section (Figure 6(c)). As λ decreased to 0.25 kJ/m, the balling effect on SLM-processed surface became worsened. Two categories of balling phenomena occurred in this case: (1) large-sized, spherical shaped agglomerates with an average size of ~500 μm; and (2) a large amount of relatively small, micrometer-scaled balls formed around these large agglomerates (Figure 6(b)). The aggravation of balling effect resulted in the formation of the interconnected interball pore channels on the top surface (Figure 6(b)) and the heterogeneous cross-sectional microstructure consisting of uneven SLM layers and large-sized, irregular-shaped interlayer pores (Figure 6(d)).

B. *Microstructure Development*

The characteristic microstructures of the first kind of ball-milled TiC/Ti nanocomposite powder under different SLM conditions are shown in Figure 7. The figure reveals that the TiC-reinforcing phase typically had a lamellar microstructure which was completely different from the starting particulate morphology before SLM (Figure 1(d)). A quantitative measurement during FE-SEM analysis showed that the thickness of such lamellar TiC reinforcement was generally below 100 nm, while the values of length were distributed from 500 nm to 1.2 μm (Figure 7). It is known that nanomaterials are materials that have structured components with at least one dimension less than 100 nm.[40] According to this definition, it was confirmed that the TiC reinforcement in SLM-processed TiC/Ti nanocomposites under these four different SLM processing conditions generally had a standard nanostructure. In addition, the ultrafine nanoscale TiC-reinforcing phase was dispersed homogeneously throughout the Ti matrix. Except for these common microstructural features, a close examination of microstructures revealed that the TiC reinforcement also demonstrated its individual unique characteristics with variation of laser energy density (λ). The nanostructure of TiC-reinforcing phase at the relatively high λ (Figures 7(a) and (b)) showed a slight coarsening and aggregation relative to the TiC reinforcement formed at lower λ (Figures 7(c) and (d)).

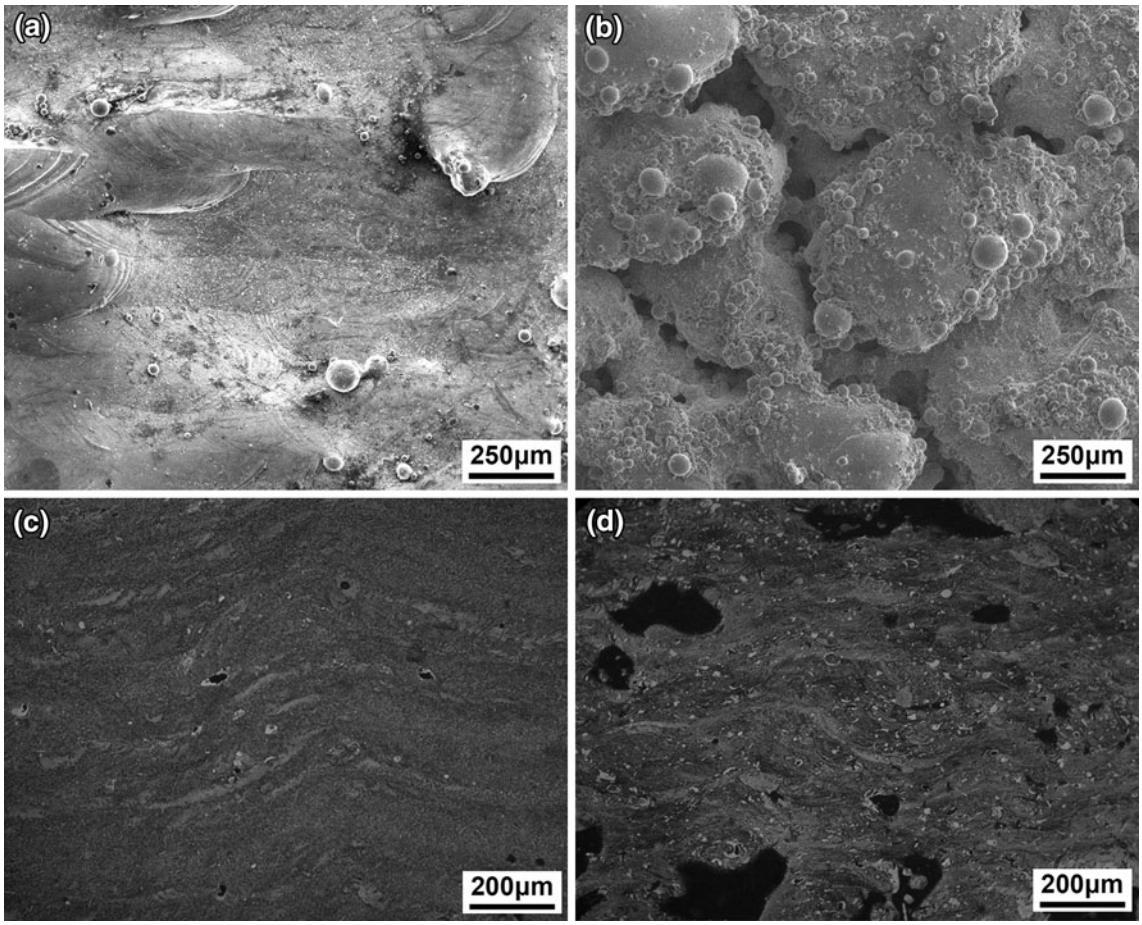

Fig. 6—Typical surface morphologies (SEM) and cross-sectional microstructures (OM) of SLM-processed parts using second kind of directly mixed TiC/Ti nanocomposite powder: $\lambda = 1.0$ kJ/m, $v = 0.1$ m/s (*a* and *c*); $\lambda = 0.25$ kJ/m, $v = 0.4$ m/s (*b* and *d*).

Nevertheless, the lamellar nanostructure and dispersion homogeneity of TiC-reinforcing phase in SLM-processed ball-milled TiC/Ti nanocomposites did not show a substantial change with the applied SLM processing parameters.

The changes of the microstructural features of the second kind of directly mixed TiC/Ti nanocomposite powder at various SLM processing parameters are provided in Figure 8. It revealed that the microstructures of the TiC reinforcement in the current study showed a distinct variation with the applied laser energy density (λ). As a reasonable λ value of 0.33 kJ/m was settled for, the ultrafine lamellar nanostructured TiC reinforcement was dispersed uniformly in the SLM-processed part (Figure 8(c)). Such a microstructure was similar to that formed in the SLM-processed ball-milled TiC/Ti nanocomposite powder (Figure 7). As the applied λ increased to 0.5 kJ/m, the TiC-reinforcement phase became apparently coarsened and, meanwhile, aggregated into clusters (Figure 8(b)). At an even higher λ value of 1.0 kJ/m, the TiC reinforcement typically exhibited dendritic growth morphology and network distribution. The average lengths of dendrite trunks and primary dendrite arms reached 2.8 μm and 0.8 μm, respectively, typically showing a micrometer-scaled feature (Figure 8(a)). In this situation, the TiC reinforcement lost its nanostructure after SLM process. It was accordingly concluded that the microstructural development of the directly mixed TiC/Ti nanocomposite powder during SLM was more sensitive to the applied laser-processing parameters.

C. *Tribological Property*

The effects of the category of nanopowder and corresponding SLM parameters on the tribological property of SLM-processed parts are depicted in Figure 9. For the SLM part condensed from the first kind of ball-milled TiC/Ti nanocomposite powder, the COF was considerably high as a relatively low λ value of 0.25 kJ/m was applied, with the average value reaching 0.52. For the higher λ value from 0.33 to 1.0 kJ/m, the mean COF decreased at least by half, which changed slightly from 0.25 to 0.22 (Figure 9(a)). The resultant wear rates of SLM parts demonstrated a similar variation tendency as the COF. An insufficient λ of 0.25 kJ/m resulted in a high wear rate of 5.3×10^{-16} $m^3\ N^{-1}\ m^{-1}$. An increase in λ above 0.33 kJ/m lowered the wear rate significantly, and the values were within the range of 2.8×10^{-16} to 3.1×10^{-16} $m^3\ N^{-1}\ m^{-1}$ (Figure 9(b)).

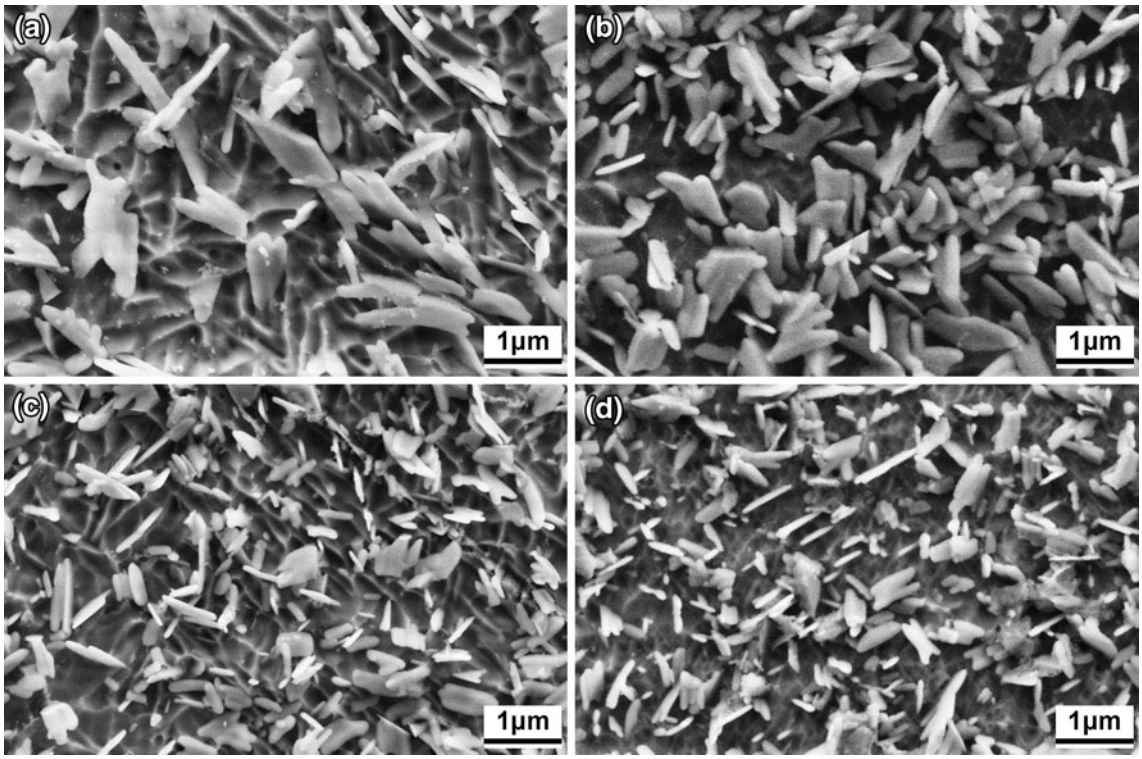

Fig. 7—FE-SEM micrographs showing the influence of SLM parameters on microstructural characteristics of nanoscale TiC-reinforcing phase in SLM-processed parts using first kind of ball-milled TiC/Ti nanocomposite powder: (*a*) $\lambda = 1.0$ kJ/m, $v = 0.1$ m/s; (*b*) $\lambda = 0.5$ kJ/m, $v = 0.2$ m/s; (*c*) $\lambda = 0.33$ kJ/m, $v = 0.3$ m/s; (*d*) $\lambda = 0.25$ kJ/m, $v = 0.4$ m/s.

As to the second category of nanopowder, the average COFs and attendant wear rates of SLM-processed parts were generally higher than that of SLM parts using the ball-milled TiC/Ti nanocomposite powder (Figure 9), which implied the relatively low tribological property and antiwear performance of the parts consolidated from the directly mixed TiC/Ti nanocomposite powder. The influence of λ on the COF and wear rate showed its unique characteristics in this instance. Similar as the SLM-consolidated ball-milled TiC/Ti nanocomposite powder, the average COF of 0.61 and resultant wear rate of 5.8×10^{-16} m^3 N^{-1} m^{-1} were highest at a relatively low λ of 0.25 kJ/m. Differently, as the applied λ increased from 0.33 to 1.0 kJ/m, the average COF increased markedly from 0.28 to 0.48 (Figure 9(a)), resulting in a significant elevation of wear rate from 3.2×10^{-16} to 4.9×10^{-16} m^3 N^{-1} m^{-1} (Figure 9(b)). Furthermore, it was noted that for the given powder system and λ, the wear rate of the SLM-processed TiC/Ti nanocomposites generally showed a decrease as the obtained COF decreased (Figure 9).

The high-magnification FE-SEM characterization was performed to study the morphologies of worn surfaces, in order to disclose the underlying microstructures responsible for the variation of tribological property. For the directly mixed TiC/Ti nanocomposite powder, the worn surface of SLM-processed part at a relatively high λ of 1.0 kJ/m was porous and consisted of loose and coarsened grains with a mean size of 450 nm (Figure 10(a)). The formation of the coarsened dendritic microstructure and resultant disappearance of nanostructured TiC reinforcement in this case (Figure 8(a)) were regarded as the direct factor in producing the coarse-grained worn surface (Figure 10(a)) with a limited antiwear performance (Figure 9). As the applied λ decreased to 0.5 kJ/m, the worn surface became dense on a microscopic scale and the average grain size decreased to 250 nm (Figure 10(b)). Interestingly, at an even lower λ of 0.33 kJ/m, the worn surface consisted of significantly refined grains with the sizes generally less than 200 nm (Figure 10(c)). In this situation, the favorable nanostructured TiC reinforcement was produced after SLM (Figure 8(c)), which in turn favored the grain refinement within the worn surface (Figure 10(c)) and the enhancement of tribological property (Figure 9).

IV. DISCUSSION

A. *Mechanisms of Densification and Microstructural Development*

As a high-energy laser beam scans over the powder bed, the energy is absorbed by powder particles via both bulk-coupling and powder-coupling mechanisms.[41] In an initial step, the energy is absorbed in a narrow layer of individual particles determined by the bulk properties of the materials, producing a high temperature on particle surfaces during the interaction. After thermalization of the energy, heat flows mainly toward the center of particles until a local steady state of the temperature is obtained within the laser irradiated area.

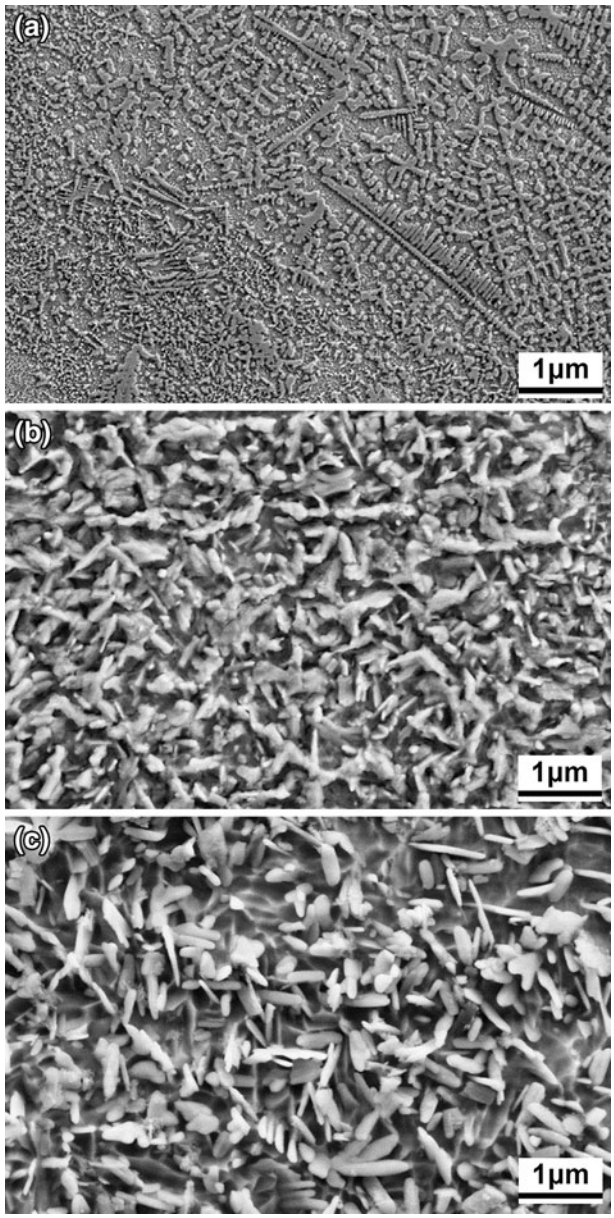

Fig. 8—FE-SEM micrographs showing the effect of SLM parameters on microstructural developments of TiC reinforcing phase in SLM-processed parts using the second kind of directly mixed TiC/Ti nanocomposite powder: (*a*) $\lambda = 1.0$ kJ/m, $v = 0.1$ m/s; (*b*) $\lambda = 0.5$ kJ/m, $v = 0.2$ m/s; (*c*) $\lambda = 0.33$ kJ/m, $v = 0.3$ m/s.

A further thermal development tends to melt the powder and produce a molten pool. As SLM is processed via a complete melting metallurgical mechanism, even the high-melting-point TiC phase tends to be fully molten during SLM. The as-used TiC nanoparticles in this study demonstrate a high tendency for complete melting due to: (1) the application of fiber laser having high energy density and resultant elevated SLM temperature; and (2) the significantly elevated activity of nanoparticles induced by the extremely large surface area to volume ratio. A molten pool with a complete liquid formation is thus generated. The dynamic viscosity (μ) of the melt within the pool can be estimated by

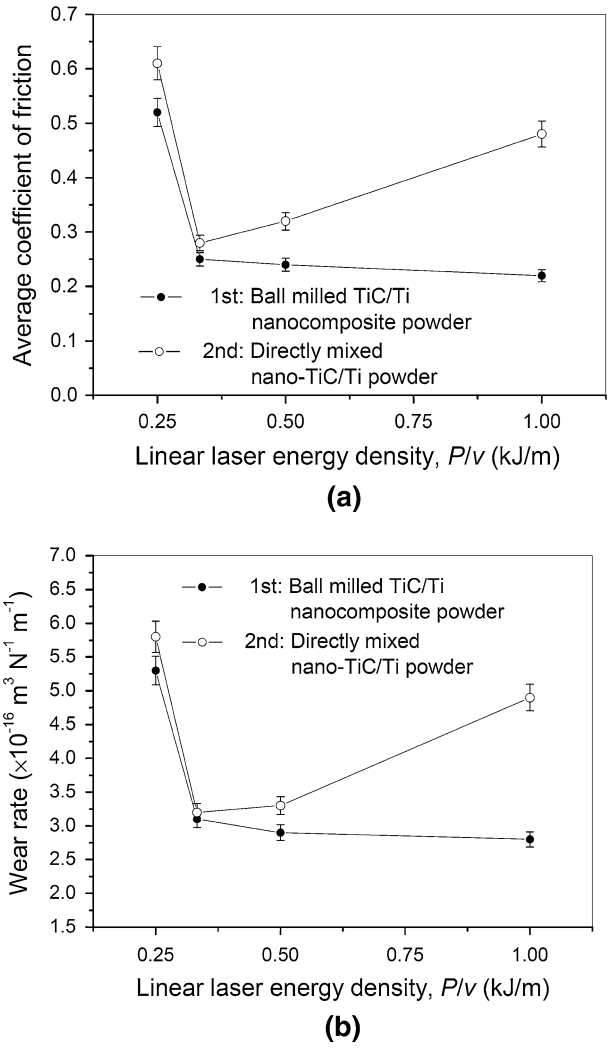

Fig. 9—Changes of average COF (*a*) and wear rate (*b*) of SLM-processed TiC/Ti nanocomposite parts with powder categories and SLM parameters.

$\mu = \frac{16}{15}\sqrt{\frac{m}{kT}}\gamma$, where m is the atomic mass, k the Boltzmann constant, T the temperature, and γ is the liquid surface tension.[42] The γ of TiC in pure molten state is ~10 to 20 N/m,[43] which is considerably larger than that of Ti liquid (1.588 N/m).[44] With the dissolution of molten TiC in Ti liquid, the viscosity of TiC/Ti composite melt may increase significantly. Furthermore, the viscosity of the melt is temperature dependant, as revealed in the above equation. As the applied laser energy density λ decreases, the operating SLM temperature T decreases, resulting in the elevation of μ. Therefore, both the TiC/Ti composite material's nature and the insufficient laser energy input tend to enhance the melt viscosity, thereby decreasing the wetting characteristics of the melt within the pool. Furthermore, during SLM process, a steep thermal gradient is developed between the center and edge of the pool across the surface, giving rise to the surface tension gradient and attendant Marangoni convection within the pool.[45] The combined influence of Marangoni flow and limited wettability causes the melt to spheroidize,

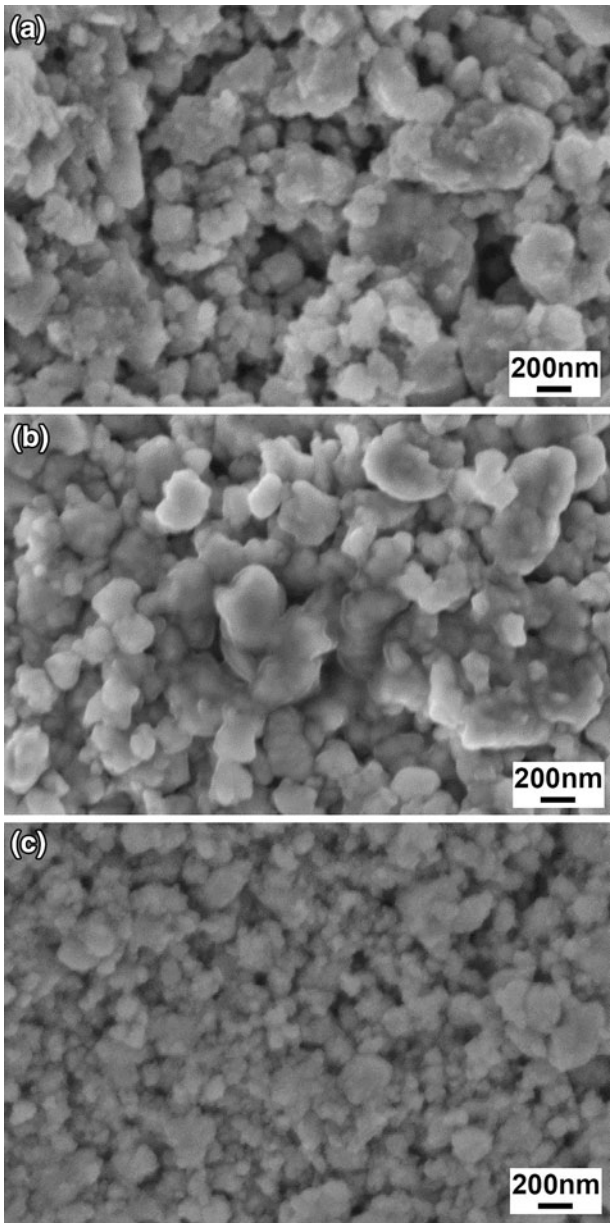

Fig. 10—FE-SEM images showing typical microstructures on worn surfaces of SLM-processed parts using the directly mixed TiC/Ti nanocomposite powder and various SLM parameters: (*a*) $\lambda = 1.0$ kJ/m, $v = 0.1$ m/s; (*b*) $\lambda = 0.5$ kJ/m, $v = 0.2$ m/s; (*c*) $\lambda = 0.33$ kJ/m, $v = 0.3$ m/s.

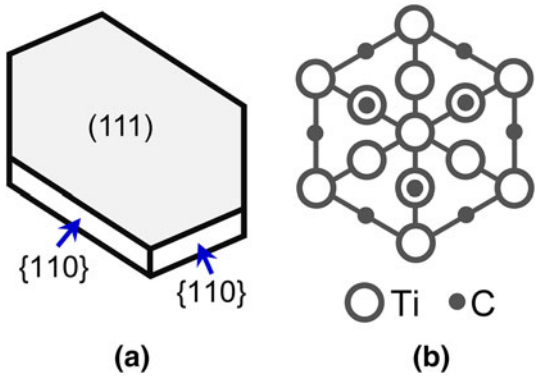

Fig. 11—Crystal structure of TiC (*a*) and projection of Ti and C atoms along [111] orientation (*b*).

rather than spreading outward on the underlying surface.[46] Balling effect, consequently, occurs on the surfaces of SLM-processed TiC/Ti parts using a low laser energy density (Figures 5(b) and 6(b)). Balling effect tends to produce a large amount of interball and intertrack porosity as a current layer is processed (Figures 5(b) and 6(b)). Also, during layer-by-layer AM process, balling effect is detrimental to the smooth spreading of the fresh powder on the previously processed layer. When such an uneven powder layer undergoes the laser fusing, the melting/solidification front of a moving molten pool is easy to be interrupted, producing the residual pores between the uneven SLM layers (Figures 5(d) and 6(d)). It is accordingly reasonable to conclude that the occurrence of balling phenomena caused by an insufficient laser energy input is a key factor in influencing the SLM densification of TiC/Ti nanocomposite powder.

On the other hand, the TiC-reinforcing phase in SLM-processed TiC/Ti nanocomposite parts generally has a unique nanostructure which is distinctly different from the starting nanoparticle morphology before SLM (Figures 1(d) and 2(a)), which is regarded as a direct evidence for the occurrence of the complete melting and subsequent crystallization of TiC during SLM. As mentioned above, SLM is processed through a full melting/solidification manner and, therefore, the TiC is formed through a dissolution/re-precipitation mechanism via the heterogeneous nucleation of TiC nuclei and subsequent grain growth. As the suitable SLM conditions are determined, the TiC reinforcement typically demonstrates a lamellar nanostructure with a nanoscale thickness (Figures 7 and 8(c)). Its formation is attributed to the combined effects of the crystal structure of TiC and the unique metallurgical nature of laser processing. TiC is a typical, faceted crystal. If viewed along the direction perpendicular to the (111) planes, Ti and C atoms form a hexagonal shape, as shown in Figure 11(b). The basal plane of TiC platelet is the (111) facet and side surfaces are {110} facets, as illustrated in Figure 11(a). Under the complete liquid condition in the molten pool, the TiC nuclei are free from restriction and are easy to form hexagonal platelet nuclei. The TiC nuclei then grow from the liquid and the crystal structure is determined by the relative growth rates on the different planes. The development of lamellar TiC in this study reveals that the growth rate on the TiC (111) facet is slow, while the speed on the {110} side facets is fast. Furthermore, laser melting involves a highly non-equilibrium rapid solidification process and laser-induced cooling rate can reach a high value of 10^{6-7} K/s.[16] Under this condition, the TiC platelet nuclei with a (111) basal plane has an insufficient time for grain growth, well retaining the considerably refined nanometric nature of the TiC reinforcement. Furthermore, it is worth noting that the ultrafine nanoscale-reinforcing phase, although it inherently has a high tendency for aggregation, is

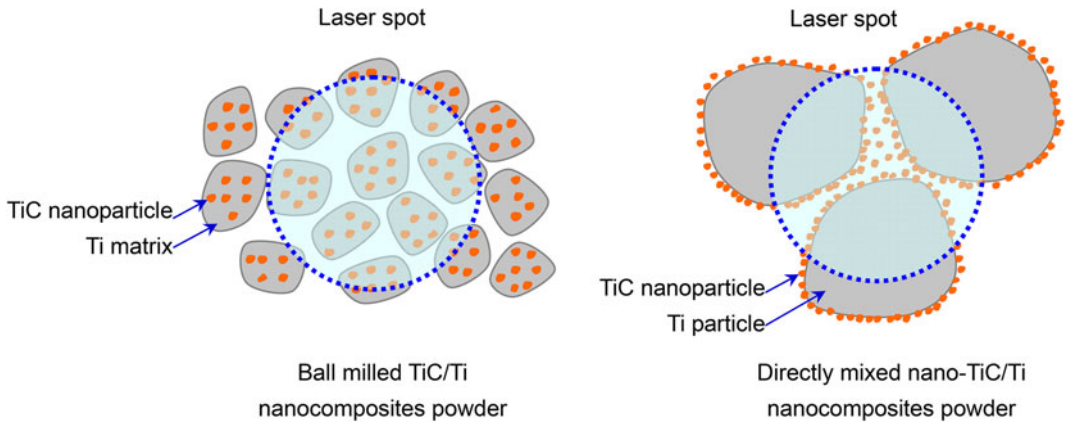

Fig. 12—Schematic of interaction mechanisms of laser beam with the two kinds of TiC/Ti nanocomposite powder.

dispersed homogeneously throughout the matrix under the optimal SLM conditions (Figures 7 and 8(c)), due to the unique Marangoni effect induced by high-energy laser melting. The Marangoni flow, as a convective stream within the molten pool, tends to induce liquid capillary force, which in turn exerts on the precipitated TiC nuclei. The rearrangement rate of the TiC in the liquid is thus elevated, thereby homogenizing its dispersion state throughout the laser-processed nanocomposites.

B. *Influence of Nanopowder Characteristics*

Besides the above mentioned general mechanisms of SLM densification and microstructural development, the present study reveals that the preparation and characteristics of nanopowder have some significant effects on these mechanisms. As schematically depicted in Figure 12, the as-used two kinds of TiC nanoparticles experience the different laser irradiation mechanisms during laser-powder interaction. For the ball-milled TiC/Ti nanocomposite powder, the TiC nanoparticles are dispersed uniformly in the interior of Ti matrix (Figure 1(d)). Therefore, in the initial stage of laser melting, the TiC nanoparticles do not expose directly to laser irradiation (Figure 12(a)). The dissolution of the TiC lags behind the melting of Ti. With the sufficient wetting of the surrounding Ti liquid, the TiC nanoparticles become melted in laser-irradiated molten pool, followed by a re-precipitation process to form the desired nanostructure. As the melting and crystallization of TiC nanophase are free from the direct interaction of laser beam, the influence of SLM parameters on the microstructural development is not significant. The lamellar nanostructure of the TiC reinforcement in SLM-processed nanocomposites can be maintained within a wide range of SLM parameters (Figure 7). Differently, for the directly mixed nano-TiC/Ti nanocomposite powder, the TiC nanoparticles are distributed around the Ti powder surface (Figure 2(c)) and, accordingly, the laser beam acts on the TiC nanoparticles directly (Figure 12(b)). The TiC nanoparticles undergo a simultaneous melting as the Ti powder. In the area exposed to the laser beam, the effect of evaporative recoil on the melt is significant and the resultant dynamic recoil pressure tends to exert an effective disturbance on SLM behavior of TiC nanophase.[47] The balling effect, which is essentially caused by the melt instability,[3,39] is more serious in this instance (Figure 6(b)), thereby decreasing the obtainable densification level (Figure 4). Also, the precipitated TiC nuclei tend to receive a more significant kinetic instability and turbulence on a microscopic scale. Consequently, the microstructures of SLM-processed directly mixed TiC/Ti nanocomposite powder are sensitive to the applied SLM parameters and the TiC reinforcement experiences a successive variation from the nanoscale lamellar structure to the relatively coarsened dendritic microstructure as the laser energy density increases (Figure 8). Furthermore, the different powder morphology (size and shape) of as-prepared two kinds of powders also influences the final SLM microstructures. As relative to the directly mixed nano-TiC/Ti powder system, the homogeneity of particle structure and size distribution of the ball-milled TiC/Ti composite powder shows a significant enhancement (Figures 1(c) and 2(c)). The interaction of the laser beam with the milled powder, accordingly, becomes much smoother, leading to a steadier laser melting process and fewer disturbances in the crystallization and development of TiC nanostructures (Figure 7).

C. *Relationship of Densification, Microstructure, and Tribological Performance*

The present study reveals that the SLM-processed TiC/Ti nanocomposite parts under optimal processing conditions have near full density and superior tribological performance. As relative to the pure Ti parts produced using SLM in our previous study,[15] the COF of TiC/Ti nanocomposites decreased about 77 pct and the resultant wear rate lowered at least 80 pct. In order to disclose the underlying mechanisms contributed to the performance enhancement, a comprehensive relationship of as-used nanopowder, SLM process, microstructures, and mechanical properties is determined. First, the densification rate of SLM parts plays a basic role in determining the tribological property. At the

relatively low laser energy input, although the TiC reinforcement exhibits the favorable nanostructure (Figure 7(d)), the SLM densification response is limited due to the pores formation caused by balling effect (Figures 4 through 6), resulting in a significant increase in the COF and wear rate (Figure 9).

Second, only when the nanostructure of the TiC reinforcement is maintained after SLM, can the tribological performance of SLM parts be maximized. For the ball-milled TiC/Ti nanocomposite powder, the nanoscale lamellar TiC reinforcement is formed within a wide range of laser energy densities (Figures 7(a) through (c)). During sliding wear tests, the homogeneously dispersed ultrafine TiC nanophase is not easy to be split, but has a high tendency to stick to each other, due to the considerably small interfacial stresses of nanoscale-reinforcing phase with the matrix.[48] As the counterface ball slides against the surface, the worn surface experiences a sufficient plastic deformation at a temperature below its recrystallization temperature. A hardened sliding-treated layer consisting of significantly refined grains is thus produced on the wear surface (Figure 10(c)), which favors the enhancement of wear resistance. In contrast, for the directly mixed nano-TiC/Ti powder, the nanostructured TiC reinforcement is not maintained in SLM part using a high energy density (Figure 8(a)). Although the SLM densification level is sufficiently high in this instance (Figures 4 and 6(c)), the present relatively coarsened dendritic TiC reinforcement (Figure 8(a)) is easy to be fragmented during sliding, thereby producing a porous wear surface having coarsened grains (Figure 10(a)) and limited tribological property (Figure 9).

V. CONCLUSIONS

The AM of bulk-form TiC/Ti nanocomposite parts was performed using SLM technology. The main conclusions were summarized as follows.

1. The densification behavior of TiC/Ti nanocomposite parts was controlled by both laser processing conditions and powder preparation method. Using an insufficient laser energy density of 0.25 kJ/m lowered the SLM densification rate, due to the occurrence of balling effect. An increase in the laser energy density from 0.33 to 1.0 kJ/m produced near fully dense SLM parts. The SLM densification level of the ball-milled TiC/Ti nanocomposite powder showed an improvement of 0.6 to 1.5 pct TD as relative to that of the directly mixed nano-TiC/Ti nanocomposite powder.
2. With the suitable SLM parameters determined, the TiC-reinforcing phase in SLM-processed TiC/Ti nanocomposite parts typically had a lamellar nanostructure with a nanoscale thickness, which was completely different from the starting nanoparticle morphology before SLM. The lamellar nanostructure of the TiC reinforcement in SLM-processed ball-milled TiC/Ti nanocomposite parts could be maintained within a wide range of laser energy densities from 0.25 to 1.0 kJ/m. The microstructures of SLM-processed directly mixed nano-TiC/Ti nanocomposite powder were sensitive to SLM parameters, and the TiC reinforcement experienced a successive change from the nanoscale lamellar structure to the relatively coarsened dendritic microstructure as the laser energy density increased.
3. The sufficiently high densification rate of SLM-processed TiC/Ti nanocomposite parts played a fundamental role in improving the tribological property. In combination with the formation of the nanostructured TiC reinforcement, the considerably low COF of 0.22 and wear rate of 2.8×10^{-16} m^3 N^{-1} m^{-1} were obtained. The disappearance of nanoscale reinforcement due to the presence of coarsened dendritic TiC in the SLM-processed directly mixed nano-TiC/Ti powder at a high laser energy density lowered the tribological performance considerably.

ACKNOWLEDGMENTS

The authors gratefully appreciate the financial support from the National Natural Science Foundation of China (No. 51104090), the Outstanding Youth Foundation of Jiangsu Province of China (No. BK20130035), and the NUAA Fundamental Research Funds (No. NE2013103).

REFERENCES

1. T. Vilaro, C. Colin, and J.D. Bartout: *Metall. Mater. Trans. A*, 2011, vol. 42A, pp. 3190–99.
2. J.P. Kruth, G. Levy, F. Klocke, and T.H.C. Childs: *CIRP Ann. Manuf. Technol.*, 2007, vol. 56, pp. 730–59.
3. D.D. Gu, W. Meiners, K. Wissenbach, and R. Poprawe: *Int. Mater. Rev.*, 2012, vol. 57, pp. 133–64.
4. P. Yu, M. Yan, G.B. Schaffer, and M. Qian: *Metall. Mater. Trans. A*, 2010, vol. 41A, pp. 2417–24.
5. B. Zheng, J.E. Smugeresky, Y. Zhou, D. Baker, and E.J. Lavernia: *Metall. Mater. Trans. A*, 2008, vol. 39A, pp. 1196–205.
6. B. Zheng, Y. Zhou, J.E. Smugeresky, J.M. Schoenung, and E.J. Lavernia: *Metall. Mater. Trans. A*, 2008, vol. 39A, pp. 2237–45.
7. V.D. Manvatkar, A.A. Gokhale, G. Jagan Reddy, A. Venkataramana, and A. De: *Metall. Mater. Trans. A*, 2011, vol. 42A, pp. 4080–87.
8. W.P. Liu and J.N. DuPont: *Metall. Mater. Trans. A*, 2004, vol. 35A, pp. 1133–40.
9. R. Banerjee, A. Genç, P.C. Collins, and H.L. Fraser: *Metall. Mater. Trans. A*, 2004, vol. 35A, pp. 2143–52.
10. B.V. Krishna, S. Bose, and A. Bandyopadhyay: *Metall. Mater. Trans. A*, 2007, vol. 38A, pp. 1096–103.
11. I. Yadroitsev, L. Thivillon, Ph. Bertrand, and I. Smurov: *Appl. Surf. Sci.*, vol. 254, pp. 980–83.
12. K.A. Mumtaz, P. Erasenthiran, and N. Hopkinson: *J. Mater. Process. Technol.*, 2008, vol. 195, pp. 77–87.
13. P. Fox, S. Pogson, C.J. Sutcliffe, and E. Jones: *Surf. Coat. Technol.*, 2008, vol. 202, pp. 5001–07.
14. C.Z. Yan, L. Hao, A. Hussein, and D. Raymont: *Int. J. Mach. Tools Manuf*, 2012, vol. 62, pp. 32–38.
15. D.D. Gu, Y.C. Hagedorn, W. Meiners, G.B. Meng, R.J.S. Batista, K. Wissenbach, and R. Poprawe: *Acta Mater.*, 2012, vol. 60, pp. 3849–60.
16. M. Zhong and W. Liu: *Proc. Inst. Mech. Eng. C. J. Mech. Eng. Sci.*, 2010, vol. 224, pp. 1041–60.
17. M. Das, V.K. Balla, D. Basu, S. Bose, and A. Bandyopadhyay: *Scripta Mater.*, 2010, vol. 63, pp. 438–41.

18. B. Duan and M. Wang: *MRS Bull.*, 2011, vol. 36, pp. 998–1005.
19. S.R. Athreya, K. Kalaitzidou, and S. Das: *Mater. Sci. Eng. A*, 2010, vol. 527, pp. 2637–42.
20. S. Dadbakhsh and L. Hao: *Adv. Eng. Mater.*, 2012, vol. 14, pp. 45–48.
21. S.S. Singh, D. Roy, R. Mitra, R.V. Subba Rao, R.K. Dayal, B. Raj, and I. Manna: *Mater. Sci. Eng. A*, 2009, vol. 501, pp. 242–47.
22. V. Viswanathan, T. Laha, K. Balani, A. Agarwal, and S. Seal: *Mater. Sci. Eng. R*, 2006, vol. 54, pp. 121–285.
23. A. Mortensen and J. Llorca: *Annu. Rev. Mater. Res.*, 2010, vol. 40, pp. 243–70.
24. S.K. Kumar and R. Krishnamoorti: *Annu. Rev. Chem. Biomol. Eng.*, 2010, vol. 1, pp. 37–58.
25. S.C. Tjong: *Adv. Eng. Mater.*, 2007, vol. 9, pp. 639–52.
26. M. Sherif El-Eskandarany, M. Omori, T. Hirai, T.J. Konno, K. Sumiyama, and K. Suzuki: *Metall. Mater. Trans. A*, 2001, vol. 32A, pp. 157–64.
27. I.V. Alexandrov, R.K. Islamgaliev, R.Z. Valiev, Y.T. Zhu, and T.C. Lowe: *Metall. Mater. Trans. A*, 1998, vol. 29A, pp. 2253–60.
28. P. Asadi, G. Faraji, A. Masoumi, and M.K. Besharati Givi: *Metall. Mater. Trans. A*, 2011, vol. 42A, pp. 2820–32.
29. V. Udhayabanu, K.R. Ravi, K. Murugan, D. Sivaprahasam, and B.S. Murty: *Metall. Mater. Trans. A*, 2011, vol. 42A, pp. 2085–93.
30. A.A.M. da Silva, J.F. dos Santos, and T.R. Strohaecker: *Compos. Sci. Technol.*, 2005, vol. 65, pp. 1749–55.
31. L. Xiao, W. Lu, J. Qin, Y. Chen, D. Zhang, M. Wang, F. Zhu, and B. Ji: *Compos. Sci. Technol.*, 2009, vol. 69, pp. 1925–31.
32. D.D. Gu, G.B. Meng, C. Li, W. Meiners, and R. Poprawe: *Scripta Mater.*, 2012, vol. 67, pp. 185–88.
33. D.D. Gu, Y.C. Hagedorn, W. Meiners, K. Wissenbach, and R. Poprawe: *Compos. Sci. Technol.*, 2011, vol. 71, pp. 1612–20.
34. A. Simchi, F. Petzoldt, and H. Pohl: *J. Mater. Process. Technol.*, 2003, vol. 141, pp. 319–28.
35. D.D. Gu and Y.F. Shen: *J. Alloys Compd.*, 2009, vol. 473, pp. 107–15.
36. M. Agarwala, D. Bourell, J. Beaman, H. Marcus, and J. Barlow: *Rapid Prototyping J.*, 1995, vol. 1, pp. 26–36.
37. A. Simchi, F. Petzoldt, and H. Pohl: *Int. J. Powder Metall.*, 2001, vol. 37, pp. 49–61.
38. N.K. Tolochko, S.E. Mozzharov, I.A. Yadroitsev, T. Laoui, L. Froyen, V.I. Titov, and M.B. Ignatiev: *Rapid Prototyping J.*, 2004, vol. 10, pp. 78–87.
39. D.D. Gu and Y.F. Shen: *Mater. Design*, 2009, vol. 30, pp. 2903–10.
40. P.M. Ajayan, L.S. Schadler, and P.V. Braun: *Nanocomposite Science and Technology*, 1st ed., Wiley-VCH, Weinheim, 2003.
41. P. Fischer, V. Romano, H.P. Weber, N.P. Karapatis, E. Boillat, and R. Glardon: *Acta Mater.*, 2003, vol. 51, pp. 1651–62.
42. I. Takamichi and I.L.G. Roderick: *The Physical Properties of Liquid Metals*, 1st ed., Clarendon Press, Oxford, 1993.
43. Y.T. Chan and S.K. Choi: *J. Appl. Phys.*, 1992, vol. 72, pp. 3741–49.
44. J. Tille and J.C. Kelly: *Brit. J. Appl. Phys.*, 1963, vol. 14, pp. 717–19.
45. H.J. Niu and I.T.H. Chang: *Scripta Mater.*, 1999, vol. 41, pp. 1229–34.
46. S. Das: *Adv. Eng. Mater.*, 2003, vol. 5, pp. 701–711.
47. V.V. Semak, G.A. Knorovsky, D.O. MacCallum, and R. Allen Roach: *J. Phys. D Appl. Phys.*, 2006, vol. 39, pp. 590–95.
48. L.R. Xu and S. Sengupta: *J. Nanosci. Nanotechnol.*, 2005, vol. 5, pp. 620–26.